SUPPLEMENTARY INFORMATION

Supplementary Table 1. Proxy data compilation for the IPWP region used in Fig. 1.

Reference	Type	Proxy	Site name	N (°)	E (°)
Dubois 2014	Marine core	$\delta^{13}C$	East Borneo	2.9	118.4
			Flores	-9.6	120.9
Partin 2007	Cave speleothem	$\delta^{18}O$	Gunung Buda	4.2	114.9
Chabangborn 2018	Marine core	Pollen	Core 17962	7.2	112.1
Ayliffe 2013	Cave speleothem	$\delta^{18}O$	Liang luar	-8.5	120.4
Denniston 2017	Terrestrial deposit	$\delta^{13}C$	KNI, BGC	-15.3	128.6
Dykoski 2005	Cave speleothem	$\delta^{18}O$	Dongge	25.3	108.1
Haberle 2005	Terrestrial deposit	Pollen	Lake Euramoo	-17.2	145.6
Van der Kaars 2000	Marine core	Pollen	Core SHI-9014	-5.5	126.6
Haberle 1998	Terrestrial deposit	Pollen	Tari basin	-5.8	143.0
Kealhofer 1998	Terrestrial deposit	Pollen	3KUM	17.1	103.0
Wang 2007	Marine core	Pollen	Core 18287	5.7	110.7
Yang 2020	Marine core	Pollen	CG-2	6.4	110.2
Fraser 2014	Marine core	$\delta^{18}O$ benthic, XRF, Uk37	Core MD06-3075	6.5	125.8
Hapsari 2017	Terrestrial deposit	Pollen and $\delta^{13}C$	Sungai Buluh	-1.2	103.6
Schröder 2018	Marine core	$\delta^{18}O$ benthic	22	1.4	119.1
			26	-3.6	118.2
			15	-3.6	119.4
			40	-6.9	119.6
Konecky 2016	Terrestrial deposit	$\delta^{13}C$, δD leaf wax	Tuwoti	-2.9	121.5
Niedemeier 2014	Marine core	$\delta^{13}C$, δD leaf wax	Nias	1.2	98.1
Wurster 2010	Cave guano	$\delta^{13}C$	Batu	3.2	101.7
			Palawan S	8.5	117.6
			Palawan N	10.5	119.5
Wurtzel 2018	Cave speleothem	$\delta^{18}O$	Tangga Cave	-0.35	100.75

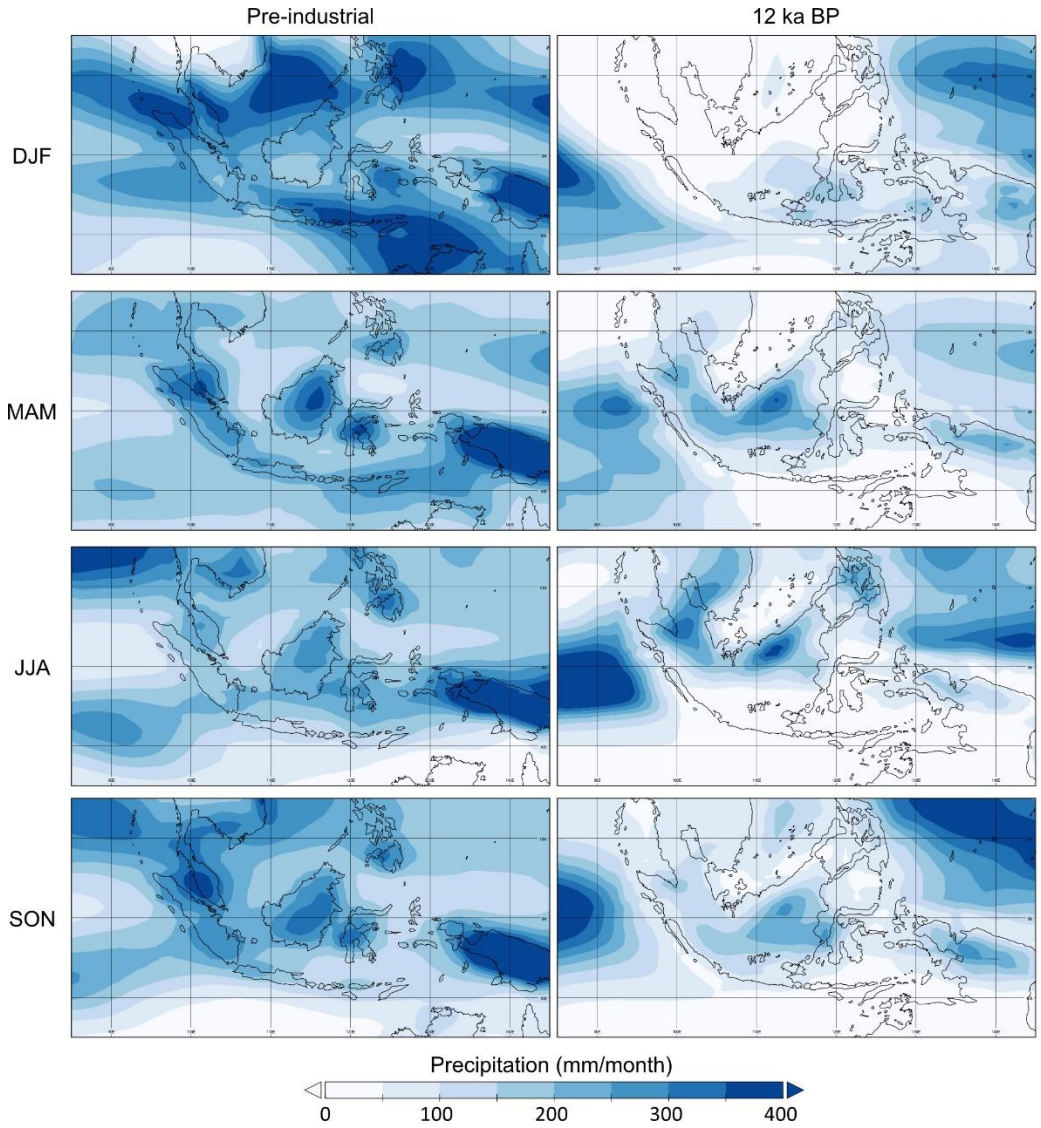

Figure S1. Simulated seasonal monthly mean precipitation (mm/month) for PI and 12 ka BP with CESM1. Coastlines at 12 ka BP are adjusted to the lower sea-level of around 55 m where roughly 70% of the Sunda Shelf were still exposed.

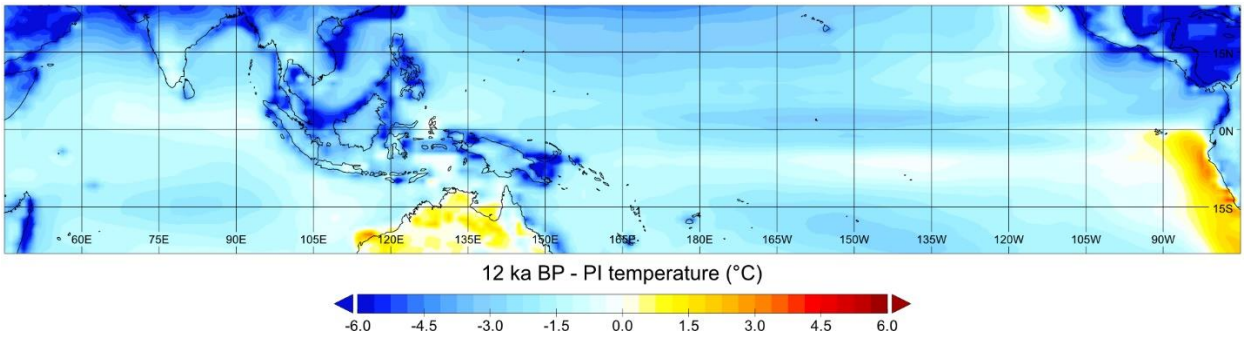

Figure S2. Annual mean surface temperature difference between 12 ka BP and PI simulated by CESM1. Red color scale indicates warmer temperatures at 12 ka BP compared to PI, blue color scale indicates cooling. The strong cooling along coastlines are partly the result of comparing land areas of 12 ka BP with ocean areas at PI due to higher sea-levels.

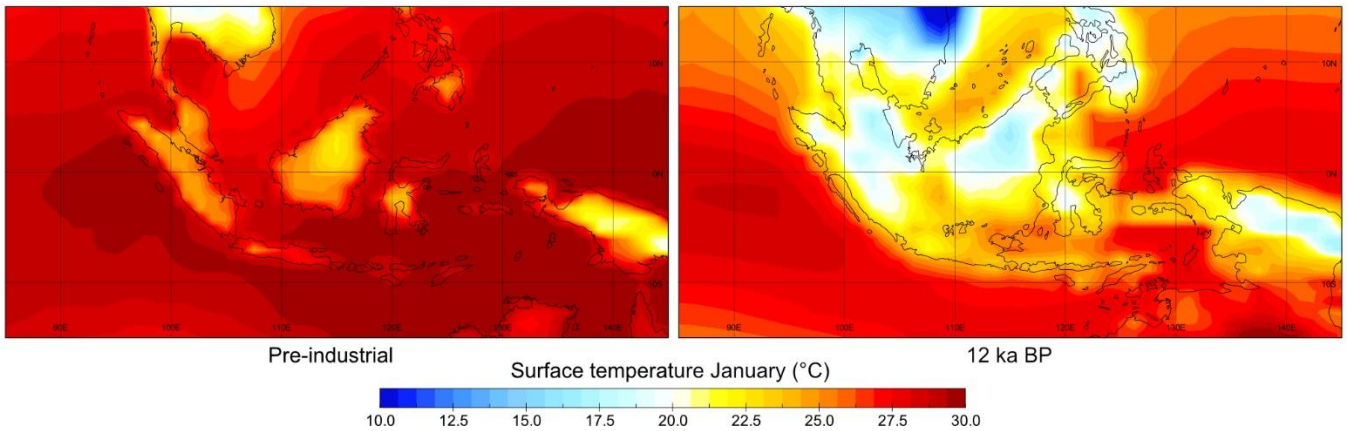

Figure S3. Mean January surface temperatures at PI and 12 ka BP simulated by CESM1. Coastlines at 12 ka BP represent the 55 m lower sea-level compared to PI. Major changes at 12 ka BP refer to much colder land areas for ISEA and the absence of today's IPWP (>28°C) region with a generally several degrees colder SST. The much stronger cooling over land than ocean at 12 ka BP promotes a reversal of the land-sea circulation with subsidence over ISEA and a breakdown of deep convection.

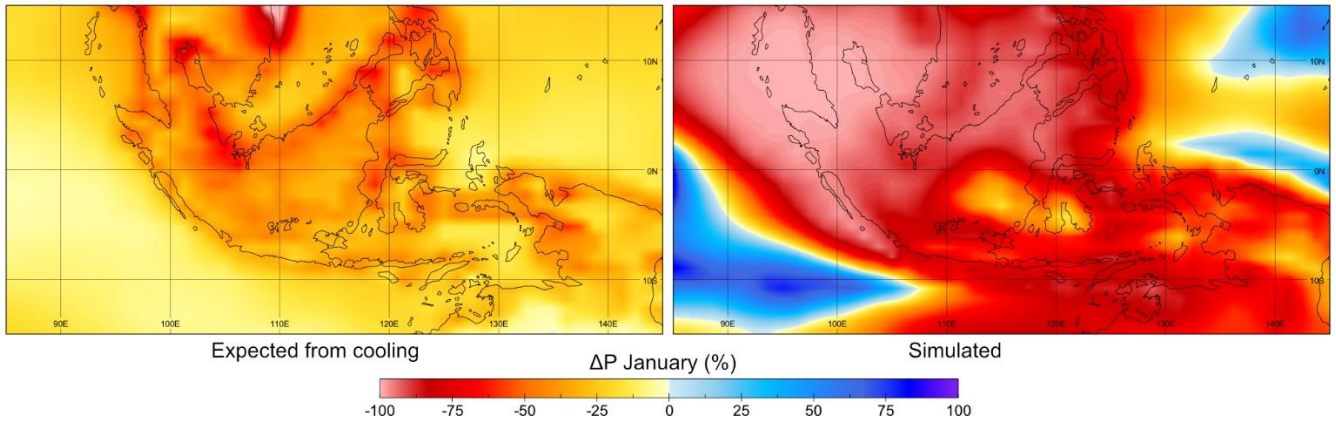

Figure S4. Comparison of theoretically expected relative precipitation change assuming a 7% decrease in P per degree cooling of $\Delta TS_{12ka-PI}$ (left) with the actually simulated total change in precipitation at 12 ka BP relative to PI (right). The example for the overall driest month at 12 ka BP (January) highlights that the reason for seasonal aridity stems mainly from dynamical rather than only thermodynamical changes.

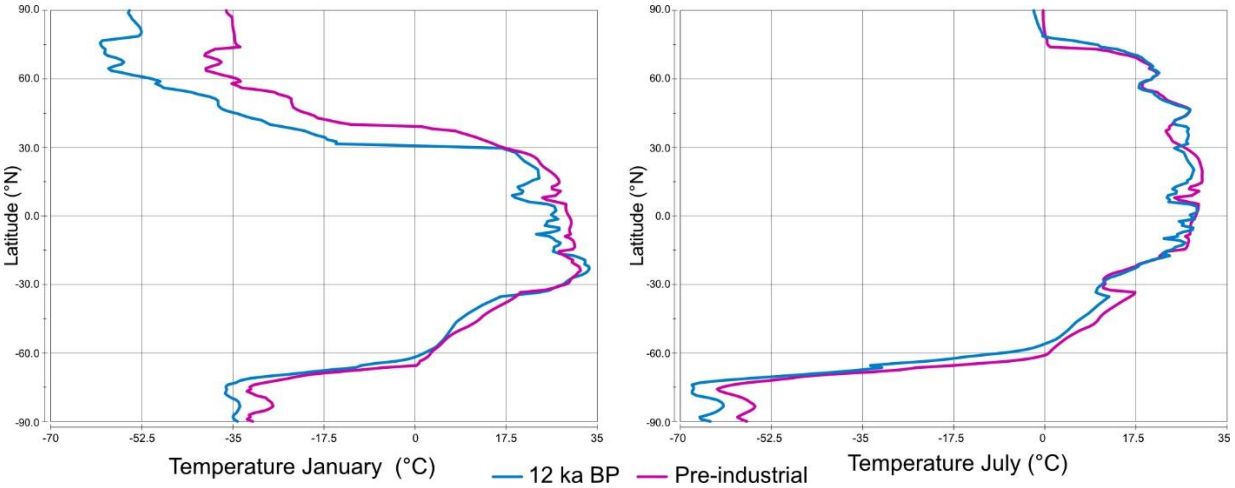

Figure S5. Comparison of zonally averaged surface temperatures for January and July along the 125 °E longitude (over Australia, Siberia and east ISEA) as simulated by CESM1 for 12 ka BP and PI. Note the large cooling north of 30°N in January for 12 ka BP which strongly increased the thermal gradient relative to the tropics as well as the interhemispheric gradient e.g. relative to the huge land mass of Australia south of ISEA. No such difference can be found in July.

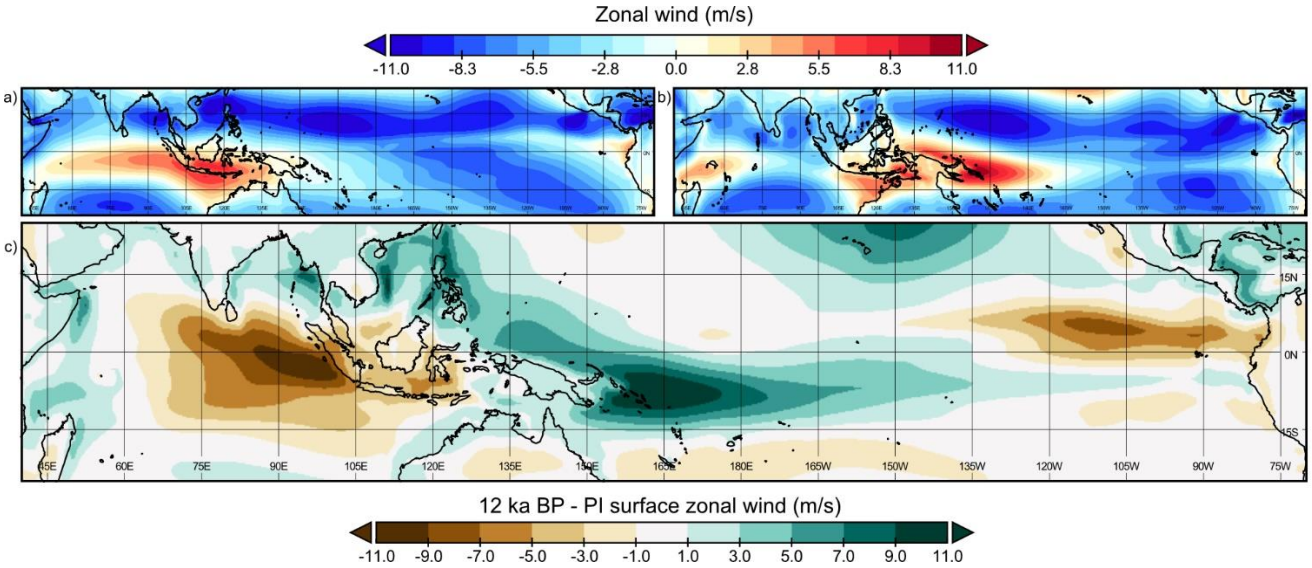

Figure S6: Comparison of zonal winds simulated by CESM1 in January for a) pre-industrial and b) 12 ka BP and c) the resulting difference in the wind vectors. Positive (red) indicate predominantly westerly winds and negative (blue) indicate easterly winds. Differences in c) between the periods with negative (brown) indicating slowdown of westerly winds, or even reversal to easterly zonal winds, and positive (green) indicate the opposite. The dipole in c) represents the reversal of the land-sea circulation to a divergent flow regime over ISEA consistent with strong terrestrial cooling of ISEA relative to the ocean in Fig. S3.

Supplementary references

1. Dubois, N. *et al.* Indonesian vegetation response to changes in rainfall seasonality over the past 25,000 years. *Nat. Geosci.* **7**, 513–517 (2014).
2. Partin, J. W., Cobb, K. M., Adkins, J. F., Clark, B. & Fernandez, D. P. Millennial-scale trends in west Pacific warm pool hydrology since the Last Glacial Maximum. *Nature* **449**, 452–455 (2007).
3. Chabangborn, A., Yamoah, K. K. A., Phantuwongraj, S. & Choowong, M. Climate in Sundaland and Asian monsoon variability during the last deglaciation. *Quat. Int.* **479**, 141–147 (2018).
4. Ayliffe, L. K. *et al.* Rapid interhemispheric climate links via the Australasian monsoon during the last deglaciation. *Nat. Commun.* **4**, 2908 (2013).
5. Denniston, R. F. Decoupling of monsoon activity across the northern and southern Indo-Pacific during the Late Glacial. *Quat. Sci. Rev.* 5 (2017).
6. Dykoski, C. *et al.* A high-resolution, absolute-dated Holocene and deglacial Asian monsoon record from Dongge Cave, China. *Earth Planet. Sci. Lett.* **233**, 71–86 (2005).
7. Haberle, S. G. A 23,000-yr Pollen Record from Lake Euramoo, Wet Tropics of NE Queensland, Australia. *Quat. Res.* **64**, 343–356 (2005).
8. Kaars, S. van der, Wang, X., Kershaw, P., Guichard, F. & Setiabudi, D. A. A Late Quaternary palaeoecological record from the Banda Sea, Indonesia: patterns of vegetation, climate and biomass burning in Indonesia and northern Australia. *Palaeogeogr. Palaeoclimatol. Palaeoecol.* **155**, 135–153 (2000).
9. Haberle, S. G. Late Quaternary vegetation change in the Tari Basin, Papua New Guinea. *Palaeogeogr. Palaeoclimatol. Palaeoecol.* **137**, 1–24 (1998).
10. Kealhofer, L. & Penny, D. A combined pollen and phytolith record for fourteen thousand years of vegetation change in northeastern Thailand. *Rev. Palaeobot. Palynol.* **103**, 83–93 (1998).
11. Wang, X., Sun, X., Wang, P. & Stattegger, K. A high-resolution history of vegetation and climate history on Sunda Shelf since the last glaciation. *Sci. China Ser. Earth Sci.* **50**, 75–80 (2007).
12. Yang, Z., Li, T., Lei, Y., Chang, F. & Nan, Q. Vegetation evolution-based hydrological climate history since LGM in southern South China Sea. *Mar. Micropaleontol.* **156**, 101837 (2020).
13. Fraser, N. *et al.* Precipitation variability within the West Pacific Warm Pool over the past 120 ka: Evidence from the Davao Gulf, southern Philippines: WPWP precipitation variability. *Paleoceanography* **29**, 1094–1110 (2014).
14. Hapsari, K. A. *et al.* Environmental dynamics and carbon accumulation rate of a tropical peatland in Central Sumatra, Indonesia. *Quat. Sci. Rev.* **169**, 173–187 (2017).

15. Schröder, J. F. *et al.* Deglacial Warming and Hydroclimate Variability in the Central Indonesian Archipelago. *Paleoceanogr. Paleoclimatology* **33**, 974–993 (2018).
16. Konecky, B., Russell, J. & Bijaksana, S. Glacial aridity in central Indonesia coeval with intensified monsoon circulation. *Earth Planet. Sci. Lett.* **437**, 15–24 (2016).
17. Niedermeyer, E. M., Sessions, A. L., Feakins, S. J. & Mohtadi, M. Hydroclimate of the western Indo-Pacific Warm Pool during the past 24,000 years. *Proc. Natl. Acad. Sci.* **111**, 9402–9406 (2014).
18. Wurster, C. M. *et al.* Forest contraction in north equatorial Southeast Asia during the Last Glacial Period. *Proc. Natl. Acad. Sci.* **107**, 15508–15511 (2010).
19. Wurtzel, J. B. *et al.* Tropical Indo-Pacific hydroclimate response to North Atlantic forcing during the last deglaciation as recorded by a speleothem from Sumatra, Indonesia. *Earth Planet. Sci. Lett.* **492**, 264–278 (2018).